Robust Low-Cost Planar Positioning Stage

For Smartphone Microscope to Diagnose Malaria in Developing Countries

M.J. Zult[1] and J. W. Spronck[1]

[1] *Department of Precision and Microsystems Engineering, Delft University of Technology*

In 2018, there were more than 200 million reported cases of malaria worldwide, most of which were in Africa. Adequate diagnostics are required to properly treat the disease. According to the WHO, microscopic examination of a blood smear is the Gold Standard of malaria diagnosis. Currently, it is a labor-intensive process requiring trained personnel, expensive equipment and a lab-environment, which makes it unsuitable for use in field environments. Most of these problems can now be tackled with a smartphone microscope, which automatically identifies malaria parasites in a bloods smear. This solution is low-cost, suitable for use in field environments and excludes the need of a trained microscopist. However, it is still a labor-intensive process: 300 unique fields of view of a blood smear must be examined and doing this by hand takes a lot of time. To solve this problem, an (semi-)automated planar positioning stage is needed, which moves the smear in 2-dof, such that 300 unique images of the surface are acquired. The stage must be low-cost, robust and suitable for field environments. At the moment, there is still a lack of such a stage. Therefore, this research aims to fill that technology gap. The stage is designed to perform a motion pattern in 300 steps, whilst ensuring that the sample remains in focus ($\delta_z \leq 50\mu m$) and that there is no overlap between images. The design encompasses a coarse motion stage stacked atop a fine motion stage (combined, it is an $R\theta$ stage. The fine motion stage consists of a compliant rotary stage actuated by a stepper motor, generating cyclic motion of 40 steps ($220\mu m$ step size). After each cycle, the hand-actuated coarse motion stage displaces the sample one step ($500\mu m$ step size). The operation is completed after 8 cycles. A demonstrator is built to investigate whether the stage meets the requirements. The 3σ step precision of both stages ensure no overlap between images ($11\mu m$ and $30\mu m$) and the 3σ focus error during operation is small ($\delta_z \leq 2\mu m$). Consequently, we have successfully designed a low-cost and robust stage capable of meeting the requirements for this application. For future work, the stepper motor can be replaced 1-on-1 by a mechanical variant, eliminating the need of a power source and electronic components, whilst significantly reducing costs.

I. INTRODUCTION

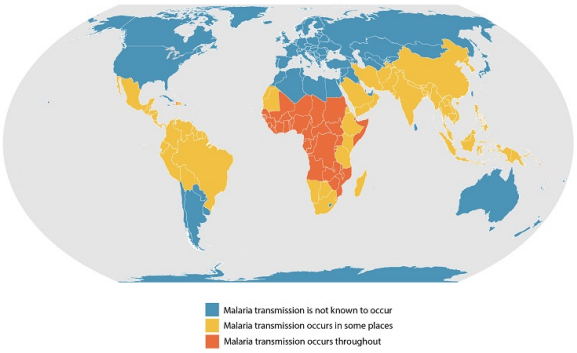

FIG. 1: Malaria Heat Map, based on data sourced by CDC [1]

In 2018, there were more than 200 million reported cases of malaria worldwide. As a result, more than 400 000 people died due to the effects of malaria that year, 67% of which were children under the age of five years [2]. Figure 1 shows the heat map of the estimated risk of malaria infection worldwide. Most of the risk is concentrated in western/central Africa. Nigeria is a textbook example, which reported 25% of malaria cases worldwide. Consequently, malaria is most problematic in remote areas in developing countries (field environments), where there is barely any access to skilled medical personnel and medical technology.

Adequate diagnostics are required, to properly treat the disease. For a reliable diagnosis, three pieces of information are vital: whether a patient is infected with malaria, the malaria parasite species and the proportion of red blood cells that are infected (the parasitemia), as indicated by the Centers for Disease Control and Prevention [3]. Currently in field environments, diagnosis is mostly done with Rapid Diagnostic Tests (RDT), which are mobile, disposable tests. Unfortunately, these can not be used on their own, as they can only indicate if a patient is infected. Consequently, these must always be used in combination with microscopy. Microscopic examination of blood smears is considered "the Gold Standard" for detecting and identifying malaria parasites by the WHO [4], as it can reliably conclude all three vital pieces of information. Sadly, microscopy is not yet suitable for use in field environments. It requires a bulky, expensive microscope, which is only available at centralized laboratories. Moreover, a trained microscopist must examine a blood smear for at least 300 fields of view (FOV) through 100X oil-immersion objective, to reliably conclude that someone does not have malaria [5].

These four challenges are tackled in the following way. The bulky microscope is replaced by a smartphone in combination with a ball lens (smartphone microscope). The smartphone microscope can automatically identify

malaria parasites in a blood smear [6] and is suitable for use in field environments: in 2015, about three quarters of Africans were in possession of a cellphone [7]. This eliminates the need of expensive equipment, trained personnel and a lab environment. There is still one challenge left: moving the smear, such that at least 300 fields of view are examined.

For that, we need a planar positioning stage, which moves the smear in 2 degrees of freedom. The stage must be robust, low-cost and suitable for use in field environments. Combined with the smartphone microscope, this results in a portable microscopic device, able to automatically perform a malaria diagnosis in field environments.

The basic concept is illustrated in figure 2. The proposed system consists of two subsystems: the optics subsystem, which consists of the smartphone, ball lens and focus mechanism, and the stage subsystem, which consists of the planar positioning stage moving the smear.

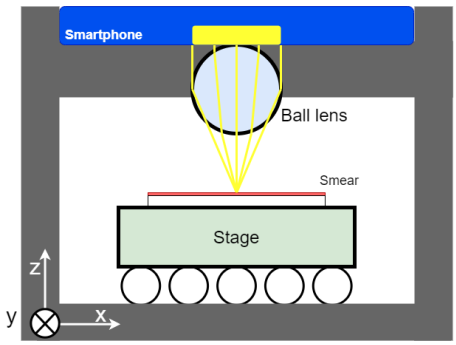

FIG. 2: Proposed concept, consisting of a smartphone + ball lens and a planar positioning stage

In the state of the art, there is a lack of a robust and low-cost stage, suitable for use in field environments. This paper aims to tackle this technology gap, so the field of microscopy can be applied effectively in developing countries, where it is needed the most. The stage is developed by first analyzing the workflow of malaria diagnosis using a smartphone microscope, from which the requirements for the stage are extracted. The resulting design is first explained on a conceptual level and then worked out in detail. A demonstrator is built, to test if the stage meets the requirements.

II. WORKFLOW ANALYSIS

The workflow of a malaria diagnosis is analyzed to obtain the requirements for the stage.

A. Smear preparation

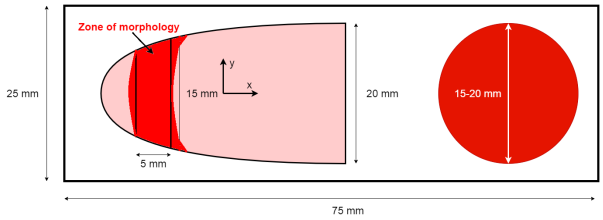

FIG. 3: Left: thin smear, right: thick smear

The process starts with the preparation of two blood smears on a standard microscopic glass slide of $25 \times 75mm$: the thick smear and the thin smear, which are shown in figure 3. The thick smear is formed by placing 1-2 drops of blood on a glass slide, which is then spread out in a circle of diameter $15 - 20mm$. To create the thin smear, a drop of blood is placed somewhere along the center line of the slide and streaked out with another slide. The resulting shape has one area which is suitable for examination: the zone of morphology. At the zone of morphology, the smear is about one cell layer thick ($2\mu m$). Consequently, a clearer view of the parasite is obtained, such that the species can be identified. The thick smear is about $50\mu m$ thick (about 20-30 cell layers). [5]. Both smears are stained with Giemsa-Stain drying.

B. Smear alignment

The smear is aligned, such that the microscope eye is located directly above the relevant surface area of the smear. This is not challenging for the thick smear, since any part of the surface is suitable for examination. This is more challenging for the thin smear, as only the zone of morphology is suitable for examination.

C. Smear examination

The thick smear is examined first, to screen for the presence of malaria parasites. A minimum of 300 fields of view (FOV) of $180 \times 180\mu m^2$ must be examined to reliably conclude a negative result. If the result is positive, the thin smear is examined, again for 300 FOV's, to conclude the parasite species and the parasitemia, which is essential information for treatment purposes. [5]. The operator examines the smear by following a scanning pattern, as shown in figure 4.

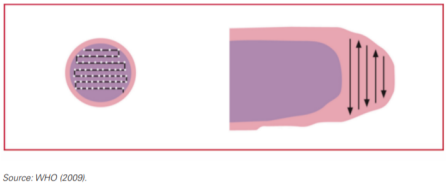

FIG. 4: Possible scanning patterns thick and thin smear (WHO 2009)

D. Requirements

The requirements are subdivided into three categories: design wishes, specified requirements and functional requirements. The design wishes shown in table I are based on the factors that come into play when designing for developing countries, acquired by running a thought experiment. When the product is manufactured, the manufacturing technologies as well as the parts must be widely available, such that it can be produced anywhere in the world (distributable). The stage must have a long lifetime and rather be maintenance-free, but if a part breaks down, it should be replaceable. To have a long lifetime, the stage must be minimally sensitive to external factors [8], such as rough handling and environmental conditions (robust). The stage must be easy to operate and easy to understand, such that anyone is able to replace parts, if needed (simple). Costs are to be minimized: proven ways to reduce costs are reducing part count, reducing assembly and fabrication time, simplifying the manufacturing process and minimizing overall dimensions (compact design) [9].

	Strategies
Robust	Durable parts/materials Replaceable parts Maintenance-free Withstand environmental conditions
Low-cost	Reduce part count Reduce assembly and fabrication time Compact design Simplify manufacturing process
Simple	Easy to operate Easy to manufacture
Distributable	Accessible parts Accessible manufacturing technologies

TABLE I: Design wishes and related strategies

The specified requirements are enumerated in table II. The range is based on the total surface area associated with 300 FOVs of $180 \times 180 \mu m^2$. During operation, the sample may not deviate more than $\pm 50 \mu m$ in z-direction, since that is the distance up to which the autofocus function of the smartphone can correct the focus. The tip/tilt ratio limit is exceeded if the stage is rotated too much about the x- or y-axis relative to the smartphone. To acquire a sharp image, the stability must be $\leq 1 \mu m$. There may be no overlap between images, since that can lead to an inaccurate parasite count and the images made of the thin smear must be of the zone of morphology, otherwise they are useless. If the requirements for the thin smear are met, the requirements for the thick smear are met as well, but not the other way around, therefore these requirements are based on the thin smear

Range	$9.72 mm^2$
Out-of-plane deviation	$\delta_z \leq \pm 50 \mu m$
Tip/tilt ratio	$\phi \leq 1.7^\circ$
Stabilty	$1 \mu m$
No overlap between images	
Zone of morphology images	

TABLE II: Specified requirements

The functional requirements are enumerated in table III. The requirements cannot be fulfilled with only linear motion, due to the shape and size of the zone of morphology, therefore guidance and actuation in 2-DOF is required. The slide must be mounted on the stage and motion in 4-DOF must be restricted.

Functional requirements
Provide guidance in 2-DOF
Provide actuation in 2-DOF
Mount the microscope slide on the stage
Constrain motion in 4-DOF

TABLE III: Functional requirements

III. CONCEPT

A. Working principle

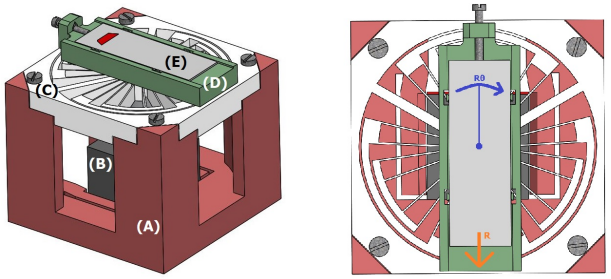

FIG. 5: Concept, consisting of (A) Frame, (B) Stepper motor, (C) Compliant rotary stage, (D) Coarse motion stage, (E) Microscope slide

The concept is shown in figure 5. The stage has a stacked structure: a fine motion stage generating a rotary back-and-forth motion ($R\theta$ - motion) and a coarse motion stage, which allows the microscope slide (the end-effector) to translate in R-direction (R - motion). Combined, this is an $R - R\theta$ stage. The fine motion stage

consists of a compliant rotary stage (C) actuated by a stepper motor (B), causing the coarse motion stage (D) to rotate, as the two are rigidly connected. The coarse motion stage consists of a screw mechanism to actuate the slide by hand. The slide functions as the stage.

The stage is designed to perform the scanning pattern illustrated in figure 6. The microscope eye is located at a distance r from the center of rotation. Thus, as the stage rotates, the experienced motion by the microscope is the curvilinear motion illustrated in figure 6, which represents one cycle of 40 steps. After each cycle, the slide is displaced one step in R-direction, such that a new part of the smear is scanned the next time. By repeating this 8 times, 320 images are acquired.

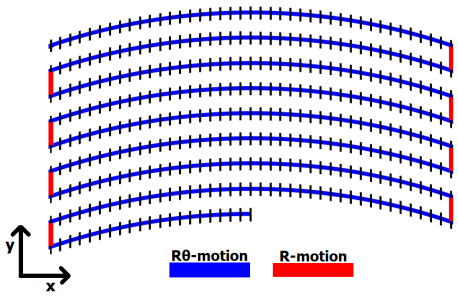

FIG. 6: Motion pattern

The shape and size of the scanning pattern is based on the zone of morphology. The slide is translated along the R-axis, until the zone of morphology is identified. Consequently, the scanning pattern is carried out. The scanning pattern has a width of 3.5 mm and a length of 8.8 mm. Therefore, there is margin in x-and y-direction of about 1.5 mm, as illustrated in figure 7. The corresponding step sizes are 220 μm in $R\theta$-direction and 500μm in R-direction. To ensure no overlap between images, which are $180 \times 180\mu m^2$, the step precision must be 20μm and 150μm, respectively.

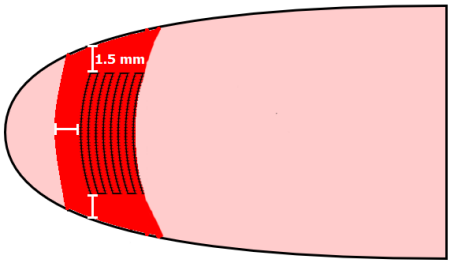

FIG. 7: Scanning pattern illustrated within zone of morphology

B. Rationale behind design choices

1. *Fine + Coarse motion*

This is based on the observation that the majority (98 %) of the steps are executed in one degree of freedom (DOF). Consequently, only the fine motion stage is automated and requires relatively more step accuracy. The coarse motion stage can be less accurate and hand-actuated, since it is only required to switch setting seven times. In this way, only one actuator is needed, resulting in a simple design and relatively low costs.

2. *Compliant rotary stage*

The compliant rotary stage is in place to ensure that the output motion is purely rotational. It only allows rotation about the z-axis and constrains the other 5 DOF. The stage achieves its motion through deformation of its own body, thus it does not experience friction and wear, as there are no sliding parts. The stage can be fabricated out of one piece, which simplifies the manufacturing process. Moreover, compliant mechanisms show repeatable motion over long time, if the stress inside the material remains below the fatigue limit. That's also where the challenge lies: the range of motion is limited by the fatigue limit, as the stage will be under cyclic loading.

3. *Stepper motor*

The stepper motor generates the desired step output and stabilizes well for image acquisition. Moreover, it operates in open-loop control and does not require a sensor. It is a reliable, low-cost and compact actuator, which operates in almost any environment. It has a long lifetime (usually about 5 years, when run 8 hours a day intensively). Stepper motors are accurate and the stepping error is non-cumulative. All in all, the stepper motor is a low-cost, easy to control and robust actuator. Last but not least, the stepper motor can potentially be replaced 1-on-1 by a mechanical variant. In this way, no power source is required and the costs can be decreased further down, as electronic components won't be needed as well. This is an option for future research and not discussed in this paper.

4. *Microscope slide motion*

A conventional microscope stage has a mounting stage to which the slide is mounted using stage clips. This concept does not differ much from the conventional stage, besides the fact that the slide is allowed to move in R-direction and there is a mechanism in place to actuate the slide along the radial axis. Therefore, it barely adds any

complexity compared to the basic mounting stage. The glass microscope slide has a hard, flat surface, making it suitable for positioning through sliding motion. Moreover, it has a small mass (5 g), so wear of the stage surface is not expected to be a problem. And last of all, if the actuation mechanism breaks down, the slide can still be positioned directly by hand, if handled accurately.

IV. DETAILED DESIGN

A. Fine motion stage

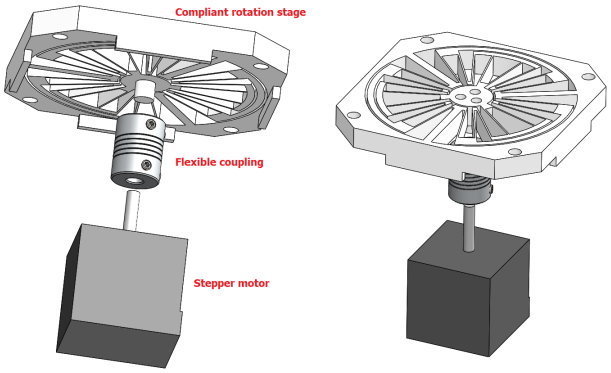

FIG. 8: Fine motion stage design

The fine motion stage design is illustrated in figure 8. The fine motion stage must attain a rotational range in 40 steps, such that a curvilinear path of 8.8 mm in horizontal width is obtained with 220 μm step size and 20 μm step precision.

1. *Stepper motor*

The NEMA17 stepper motor (0.40 Nm torque rating, 1.8 ° stepping angle) is used, which is a hybrid stepper motor. The stepper motor can operate in full-step mode, half-step mode or micro-stepping mode. Micro-stepping can be advantageous, as it runs smoother, since it has a smaller torque delivery. The smaller torque delivery can on the other hand be problematic, as sufficient torque is required to rotate the compliant stage to its most outward positions.

2. *Quarter-stepping*

The angular range and step size depend on the radial distance the smartphone camera is located from the center of rotation (the radius). Full-, half- and quarter-step mode are compared in figure 9 for a curvilinear range of 8.8 mm and a step size of 220 μm. Quarter-stepping shows the best characteristic: the angular range is feasible ($\pm 9°$) with a small enough radius ($r = 28mm$), whereas full-stepping ($\pm 18°$) and half-stepping ($\pm 36°$) require too much rotational range, which is unrealistic based on literature study. It is not opted to further decrease the step resolution, as that would require a larger radius, increasing the size of the coarse motion stage. With quarter-stepping, the torque decreases by a factor of 38%, resulting in a torque rating of 0.15 Nm.

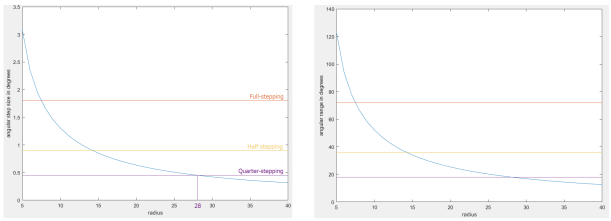

FIG. 9: Full-, half- and quarter-step mode compared

3. *Control strategy*

The stepper motor is feed-forward controlled using Arduino in combination with an A4988 stepper motor driver and a CNC shield v3. The control sequence is illustrated in figure 10. The stepper motor first performs 20 steps counter-clockwise, to the starting position. Then, it performs an alternate cycle of 40 steps clockwise and counterclockwise 4 times, with an interval of 10 seconds in between, such that the slide can be displaced. At the end, 20 steps clockwise back to rest position.

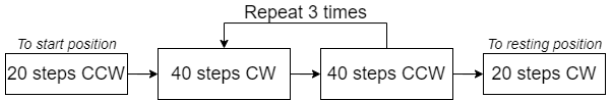

FIG. 10: Control sequence

4. *Flexible coupling*

The flexible coupling shown in figure 11 is used to connect the stepper motor with the stage, such that undesired Z-wobble motion is not transferred to the stage. The compliant stage is printed with a small shaft of 8 mm in diameter and the stepper motor has a shaft of 5 mm in diameter. A 5 mm - 8 mm flexible coupling is used to connect these two.

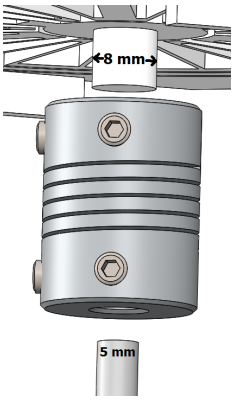

FIG. 11: Flexible coupling

5. *Compliant rotary stage*

The rotary stage is based on a design found through literature study of compliant rotary stages [10]. This design is picked, due to its large rotary range, which is required to be ±9° for this application.

The working principle of the stage is illustrated in figure 12. It consists of two radial leaf flexures. In FACT analogy [11], these two leaf flexures each form a plane and intersect on a common line (C), thus resulting in rotational motion around center line C.

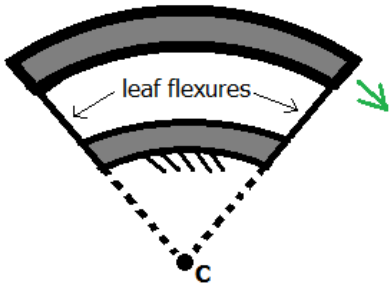

FIG. 12: Basic building block of the rotary stage

The behavior of the stage mostly depends on the flexure length, flexure thickness and flexure height, which can be concluded from the stiffness equation EQ(4.1). These variables are enumerated in table IV.

$$K = \frac{18EIR_2R_3}{L^3}, \quad I = 1/12bh^3 \tag{4.1}$$

Flexure thickness (h)	0.7 mm
Flexure height (b)	10 mm
Flexure length (L)	26 mm

TABLE IV: Flexure thickness, height and length

A CAD model of the stage is built by mirroring the segment shown in figure 13 once and then copying and shifting the resulting segment twice over 120 degrees.

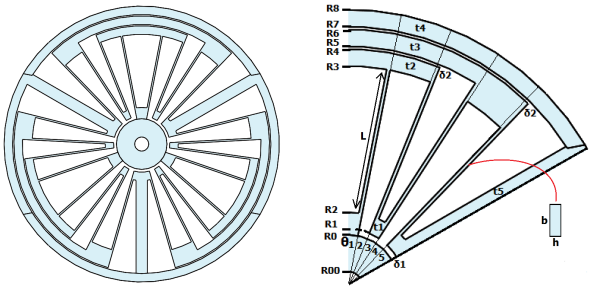

FIG. 13: Compliant rotary stage model

6. *Material selection demonstrator*

The compliant stage is fabricated with fused deposition modeling (FDM) 3D-printing. Several thermoplastic materials are investigated, to find the most suitable one. The fatigue strength is desired to be as high as possible. Constraints are implemented in the search strategy: the material must be biodegradable, the Young's Modulus (E) is bounded within 2 - 3 GPa, and the lower bound of the maximum service temperature ($T_{service}$) must be at least 56 $°C$ (10 degrees above the highest temperature ever recorded in Nigeria). Commonly used 3D-printing filaments PLA (polylactic acid), ABS (acrylonitrile butadiene styrene) and PC (polycarbonate) are compared in table V. Data is sourced from CES Edupack. PLA is unsuitable, since the maximum service temperature is too low. PC has the best material properties for the application: high maximum service temperature as well as relatively high fatigue strength. However, PC is not suitable for outdoor environments, as it is very sensitive to moisture and UV light. Therefore, ABS is the choice of material.

Material	**E** (GPa)	σ_N (MPa)	$T_{service}$ ($°C$)	Costs
ABS	2.0 - 2.9	12 - 20	63 - 77	18
PLA	2.3 - 3.5	18 - 27	45 - 55	18
PC	2.3 - 2.4	23 - 30	101 - 116	35

TABLE V: ABS, PLA and PC compared

7. *FDM-printed ABS properties*

The fatigue strength of ABS is the maximum allowable stress inside the material. Additional literature is studied to find the fatigue strength of FDM-printed ABS [12], from which is concluded that infinite fatigue life is reached, when the stress inside the material remains below 12 MPa. The Young's Modulus of an FDM-printed ABS part is obtained from literature as well [13]. These variables, as well as the density and poisson's ratio, are

used in the COMSOL study of the stage and shown in table VI.

Young's Modulus	2.4 GPa
Density	1050 kg / m3
Poisson's ratio	0.36
Maximum stress	12 GPa

TABLE VI: Properties

8. *FEM simulations*

The compliant stage is analyzed through FEM simulations. From the stress-strain curve shown in figure 14 is concluded that the material shows linear elastic behavior, below a stress level of 15 MPa. Therefore, a linear elastic material model is used in FEM simulations, a the stress may not exceed 12 MPa anyway.

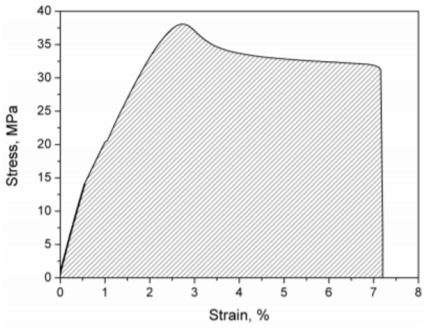

FIG. 14: Stress-strain curve FDM-printed ABS [13]

FEM simulations are done, to verify whether the stage can attain the rotational range, while staying below the fatigue limit. Moreover, if the stepper motor can deliver sufficient torque, to accomplish this. A torque input is loaded at the center of the stage, whilst the edges are fixed. A parametric sweep is used to obtain an array of data.

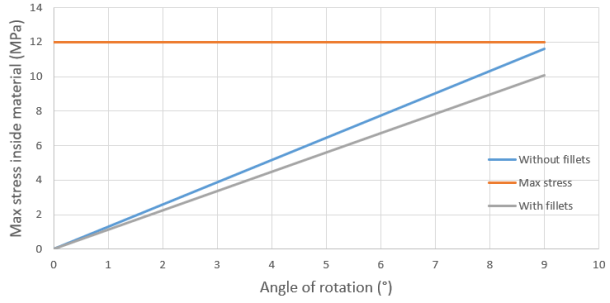

FIG. 15: Stress-rotation relation

Figure 15 shows the relation between the stress and rotation. The first results showcased a maximum stress of 11.6 MPa, which is close to the limit. Fillets were added, which lowered the maximum stress inside the material to 10.0 MPa. The addition of fillets did increase the rotational stiffness of the stage. This can be seen in figure 16, where the minimum required torque for achieving range increased from 0.08 Nm to 0.09 Nm. This is still well below the torque limit of 0.15 Nm.

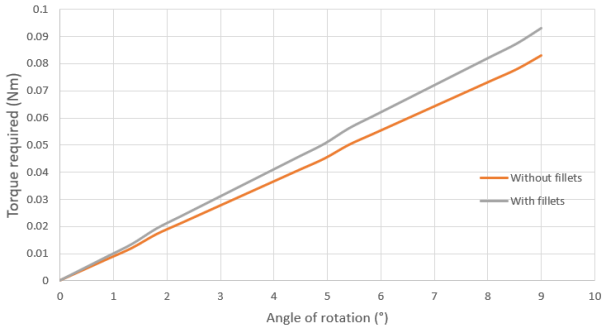

FIG. 16: Torque-rotation relation

B. Coarse motion stage

The coarse motion stage fulfills three functions: (1) actuating, (2) guiding and (3) clamping the slide. The desired step size is $500\mu m$ with a step precision $150\mu m$, to ensure no overlap between images.

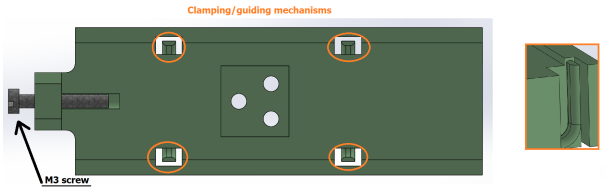

FIG. 17: Coarse motion stage top view

The coarse motion stage is shown in figure 17. An M3 screw is implemented to actuate the slide. One revolution corresponds to a step size of 500 μm, since that is the pitch of an M3 screw. If the screw wears out or corrodes, it can simply be replaced. The screw is fitted with a knob, which can lock to the stage, as shown in figure 18. This is implemented, to assist in precisely positioning the slide and to fix the screw in position, as it can rotate out of position due to the vibrations caused by the torque input of the stepper motor. A stainless steel M3 insert is placed in the front wall of the stage, relative to which the screw can rotate. There is not pretension on the slide forcing it against the slide, such as a spring. Instead, this can be done by hand, which is useful if the slide is e.g. accidentally translated a little too far.

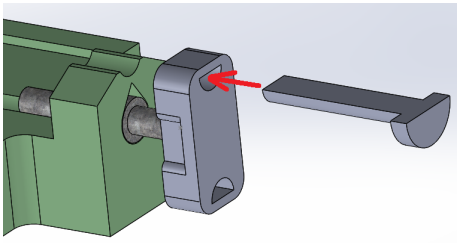

FIG. 18: Screw with knob and locking system

The slide is guided and clamped simultaneously by four compliant mechanisms, one of which is illustrated in figure 19. It's basically 4 cantilever beams applying sufficient force to clamp the slide, while still allowing guidance. The cantilever beams are designed to deflect 0.1 - 0.2 mm, remaining at a stress level of 3 - 6 MPa, which is well below the fatigue limit. The maximum deformation of the cantilever beams is limited by the edge of the coarse motion stage, such that they cannot yield. The maximum possible stress is 20 MPa, which is well below the yield strength of at least 30 MPa [CITE IETS].

For static balancing, the stage is designed, such that the center of mass of the system including the stage, M3 screw, M3 insert and microscope slide intersects with the center of rotation, while at rest (slide and screw at half their range).

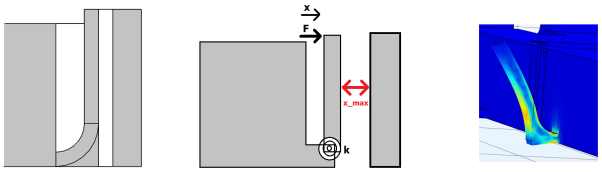

FIG. 19: Cantilever beam

It's important do discuss wear, which is the removal of material, due to sliding surfaces. Wear of the stage surface is negligible, as the slide is lightweight (5 g). Wear of the cantilever beam surfaces could be a problem, as they apply 0.1 - 0.2 N of force. Therefore, an estimation is made to investigate if it is likely to be problematic. Archard's law is generally used to describe the volume of material removed due to wear. The total volume of wear (W) depends on the normal force (F_N), the material hardness (H), the sliding distance (L_T) and a material-related constant K. K is obtained from experimental results. The sliding distance is assumed to be twice the range ($L_T = 26mm$) per smear examination. The hardness of ABS is $H = 1e8Pa$. The force is $F = 0.15N$ (average of 0.1 - 0.2). The wear coefficient is estimated at $K = 7e-6-1e-7$, based on experimental data [14]. The contact surface area is $A = 4mm^2$.

$$W_{vol} = \frac{K \cdot F_N \cdot L_T}{H} = 2.7 \cdot 10^{-7} - 3.9 \cdot 10^{-9} mm^2 \quad (4.2)$$

$$W_{depth} = \frac{W_{vol}}{A} = 6.8 \cdot 10^{-5} - 9.8 \cdot 10^{-7} \mu m \quad (4.3)$$

After $20\mu m$ of wear, the cantilever beam is deemed as failed. Consequently, depending on the conditions, the lifetime is between $N = 3 \cdot 10^5 - 2 \cdot 10^7 cycles$. If 50 analyses are done per day, this relates to a lifetime between $16 - 1100 years$.

C. Frame

The fine motion stage + coarse motion stage and the stepper motor are mounted onto the frame, which is shown in figure 20. The stage is mounted with M5 bolts and inserts. The stepper motor is clamped between two arms, which apply sufficient force, such that the stepper motor remains in place during operation.

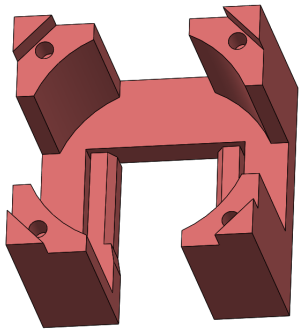

FIG. 20: Frame design

Hier iets over external vibrations?

V. FABRICATION AND ASSEMBLY

A. Demonstrator assembly

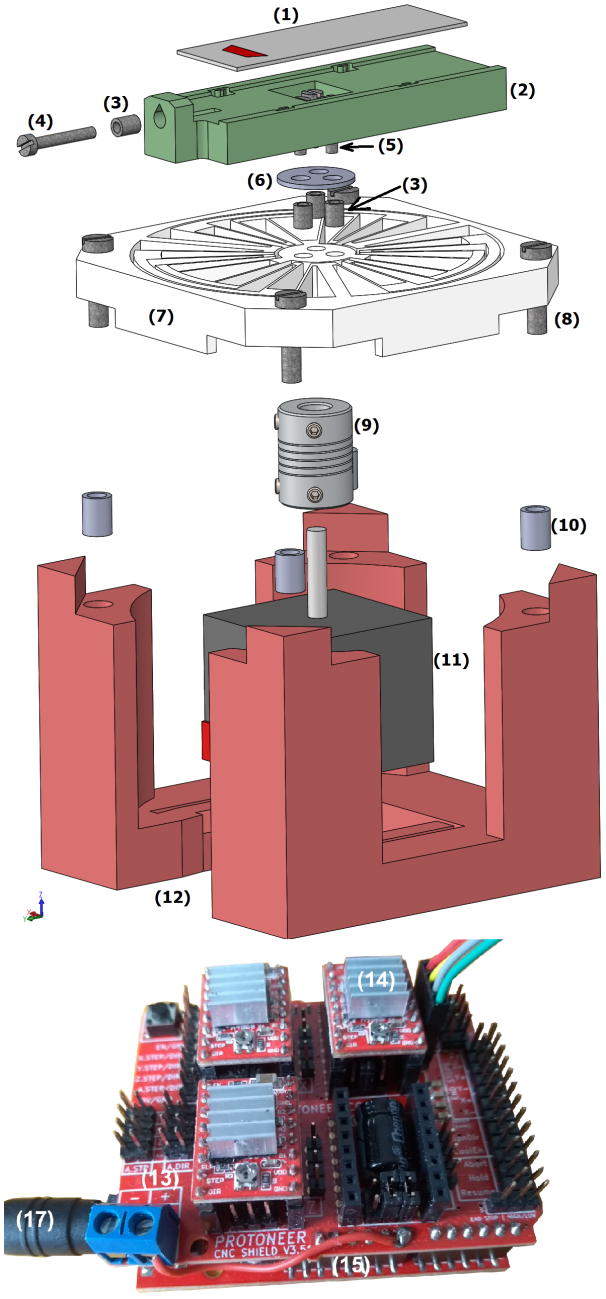

FIG. 21: Exploded view

The exploded view is visualized in figure 21 and the corresponding parts are enumerated in table VII. The coarse motion stage, fine motion stage and frame are FDM-printed out of ABS.

1. *Bulk production: Injection Molding*

Injection molded parts perform better than 3D-printed parts [13]. FDM printed parts have higher porosity, so they are likely more brittle. Injection molding is advised, when bulk production is opted for (N ¿ 10,000).

2. *Estimated costs*

Estimated costs are based on the bulk purchase of parts from large suppliers and large volume injection-molded frame and stage. The costs are enumerated in table VII. The total estimated costs range between $22,72 - $30,95, for bulk production ($15,87 - $22,95 without battery pack). Remarkable is that more than 80% of the costs are due to stepper motor related parts. We can compare the costs with RDT's, which cost about $0,15 a piece [15]. After 200 smear examinations, the costs per analysis become lower than for RDT's (excluding the costs for the optics subsystem).

#	Part	Qty	Bulk costs ($)
1	Microscope slide	1	-
2	Coarse motion stage	1	$0,80$
3	M3 insert	4	$0,04 - 0,12$
4	M3 - 20 mm bolt	1	$0,01 - 0,03$
5	M3 - 12 mm bolt	3	$0,03 - 0,09$
6	In-between piece	1	-
7	Compliant stage	1	$1,00$
8	M5 - 20 mm bolt	4	$0,04 - 0,16$
9	Flexible coupling	1	$0,58 - 0,90$
10	M5 insert	4	$0,04 - 0,12$
11	NEMA17 0.40 Nm stepper motor	1	$6,46 - 7,28$
12	Frame	1	$1,00$
13	CNC shield v3	1	$0,64 - 2,70$
14	Allegro A4988 driver	1	$0,60 - 0,94$
15	Arduino UNO	1	$2,20 - 3,05$
16	12 V Battery pack	1	$6,85 - 8,00$
17	12 V adaptor	1	$2,43 - 4,76$
	Total estimated costs		$22,72 - 30,95$

TABLE VII: Part list

B. Manufacturing tolerances

The manufacturing tolerance with 3D-printing is 0.15 mm. The manufacturing tolerance with injection molding ranges from 0.050 mm to 0.10 mm depending on the part size. The tolerances for injection molding are as follows:

Part dimensions	1 - 20 mm	21 - 100 mm
Dimensional tolerances	0.050 mm	0.10 mm

The maximum difference between two ends of a part in a worst-case scenario is 0.20 mm, which causes e.g. a

slanted surface or a height difference between two ends, both causing a bad connection between two parts. This can occur at the connection between the FMS and the frame, the CMS and the FMS, the slide and the CMS. Another potential source of error is a warped CMS surface, which causes the edges of the CMS to be 0.200 mm higher than the center.

	tip/tilt	focus, r	focus, θ
FMS - Frame			
Rotated about x	Yes	No	No
Rotated about y	Yes	No	No
CMS - FMS			
Rotated about x	Yes	No	Yes
Rotated about y	Yes	No	No
Slide - CMS			
Rotated about x	Yes	No	Yes
Rotated about y	Yes	No	No
Warped CMS	Yes	Yes	No

TABLE VIII: Sources of error and their effect on tip/tilt ratio and focus

Table VIII shows the sources of error and whether they have an effect on the tip/tilt ratio, the focus when the slide translates and the focus when the stage rotates.

1. Tip/tilt budget

The tip/tilt budget is divided into two parts: tilted with respect to the x-axis ($\epsilon_{tip/tilt,X}$) and y-axis ($\epsilon_{tip/tilt,Y}$). The limit of the two combined is 1.7°. For the connection between the FMS and the frame, there are two sources of error, which is also the case for the connection between the CMS and the frame, since both parts can have manufacturing errors.

With respect to x:

$$\begin{cases} \epsilon_{FMS-Fra,X} = \sqrt{\arcsin\frac{0.2}{100}^2 + \arcsin\frac{0.2}{100}^2} = 0.16° \\ \epsilon_{CMS-FMS,X} = \sqrt{\arcsin\frac{0.1}{15}^2 + \arcsin\frac{0.2}{25}^2} = 0.60° \\ \epsilon_{Sli-CMS,X} = \arcsin\frac{0.2}{25} = 0.46° \\ \epsilon_{CMS-Warped} = \arcsin\frac{z_{head}-z_{tail}}{75} = 0.04° \\ \epsilon_{tip/tilt,X} = \sqrt{0.16^2 + 0.60^2 + 0.46^2 + 0.04^2} = 0.77° \end{cases} \tag{5.1}$$

With respect to y:

$$\begin{cases} \epsilon_{FMS-Fra,Y} = \sqrt{\arcsin\frac{0.2}{100}^2 + \arcsin\frac{0.2}{100}^2} = 0.16° \\ \epsilon_{CMS-FMS,Y} = \sqrt{\arcsin\frac{0.1}{15}^2 + \arcsin\frac{0.2}{75}^2} = 0.41° \\ \epsilon_{Sli-CMS,Y} = \arcsin\frac{0.2}{75} = 0.15° \\ \epsilon_{tip/tilt,Y} = \sqrt{0.16^2 + 0.41^2 + 0.15^2} = 0.46° \end{cases} \tag{5.2}$$

Combined:

$$\epsilon_{tip/tilt} = \sqrt{0.46^2 + 0.77^2} = 0.90° \tag{5.3}$$

2. Focus budget

The focus budget is based on the focus error that can occur due to r- or -θ-motion, caused by manufacturing faults. We first discuss the focus error, when the stage rotates:

$$\begin{cases} \epsilon_{CMS-FMS,X} = 4 \cdot \sqrt{\frac{0.1}{15}^2 + \frac{0.2}{25}^2} = 41\mu m \\ \epsilon_{Sli-CMS,X} = 4 \cdot \frac{0.2}{25} = 32\mu m \\ \epsilon_{focus,\theta} = \sqrt{32^2 + 41^2} = 52\mu m \end{cases} \tag{5.4}$$

And when the slide translates, due to warping:

$$\epsilon_{focus,r} = 3.5 \cdot \frac{0.2}{50} = 14\mu m \tag{5.5}$$

Combined:

$$\epsilon_{focus} = \sqrt{14^2 + 52^2} = 54\mu m \tag{5.6}$$

The maximum focus error ($50\mu m$) is now exceeded. It is observed that the connection between the frame and the FMS has no effect on the focus. Therefore, the CMS and the FMS are now manufactured with the highest precision available (0.05 mm tolerance). Consequently, values of 0.2 mm in equations 5.4 and 5.5 are substituted with 0.1 mm. This yields the following results:

$$\begin{cases} \epsilon_{focus,\theta} = \sqrt{31^2 + 16^2} = 35\mu m \\ \epsilon_{focus,r} = 7\mu m \\ \epsilon_{focus} = \sqrt{35^2 + 7^2} = 36\mu m \end{cases} \tag{5.7}$$

To summarize, in a worst-case scenario, both the focus error ($36\mu m$) and the tip/tilt error (0.90°) are well below their limits ($50\mu m$ and 1.7°, respectively), if the FMS and the CMS are fabricated with the highest precision (0.05 mm tolerance) and the frame with the second-highest precision (0.10 mm tolerance).

VI. EXPERIMENTAL DESIGN AND RESULTS

Four experiments are performed to analyze the performance of the stage. The step response (experiment A), step precision of both stages (experiments B and C) and the out-of-plane displacement of the slide during operation are measured (experiment D). Two linear triangulation sensors are used to perform the measurements. For experiments A, B and C, the slide is replaced by a 3D-printed end-effector, with similar mass, but larger edges, such that the planar output motion can be measured.

A. Step response

The step response is measured, to conclude if the end-effector stabilizes (within $1\mu mband$) and what the settling time is, which has significant influence on the speed

at which the system can operate. The setup is shown in figure 22. The linear triangulation sensor measures the output motion of the end-effector, as a result of a single rotational step of the stage ($R\theta$-motion).

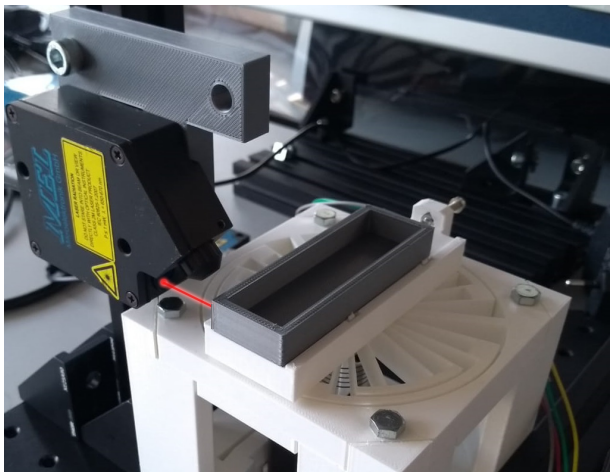

FIG. 22: Step response measurement setup

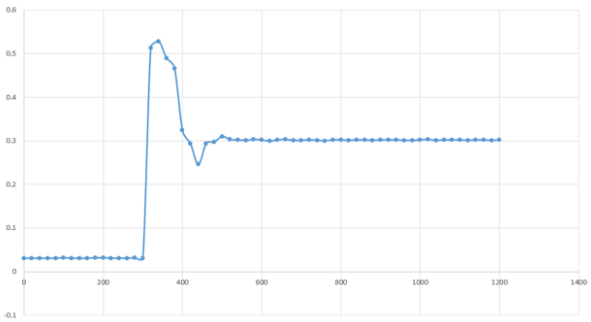

FIG. 23: Step response

Figure 23 shows one measured step response. Due to the small measurement frequency (50 Hz), the full characteristic is not shown, but it is enough information to conclude the settling time and that it stabilizes. A total of 12 step responses were done which had an average settling time of 210 ms and a 3σ value of 82 ms.

B. Precision coarse motion stage

The step size is required to be $500\mu m$ with a 3σ precision of $150\mu m$, to ensure with 99.7% certainty that there is no overlap between images. The experimental setup is shown in figure 24. The precision and accuracy are measured with a linear triangulation sensor. The screw is rotated one revolution and the translation of the end-effector is measured.

The results are set out in a normal distribution, as shown in figure 25. The measured mean step size is $500\mu m$ with a 3σ precision of $30\mu m$. Consequently, the

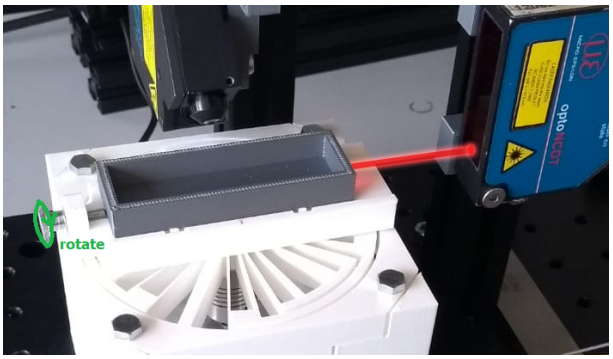

FIG. 24: Experimental setup coarse motion stage measurement

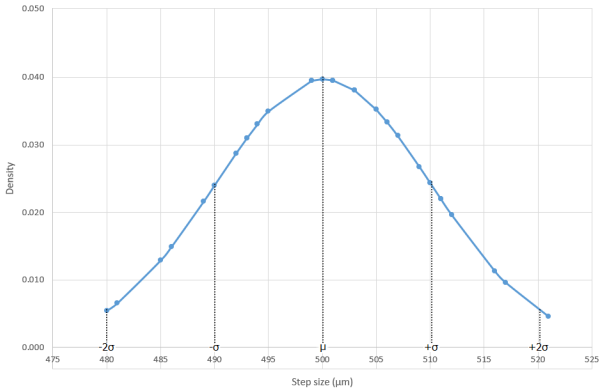

FIG. 25: Normal distribution coarse motion stage results

step size can be decreased to half a rotation ($250\mu m$ step size), which decreases the workspace from $3.5 \times 8.8mm^2$ to $1.8 \times 8.8mm^2$.

C. Step precision fine motion stage

The output step size of the fine motion stage must be $220\mu m \pm 20\mu m$. For this, the required rotational step size is 0.45°, with 3σ precision of $\pm 0.04°$, to ensure no overlap with 99.7% certainty. Two linear triangulation sensors are used to measure the angle of the stage. They are placed at a distance R_1 and R_2 from the center of rotation, which is illustrated in figure 26. The difference between Y_1 and Y_2 is used to calculate the rotational motion of the stage.

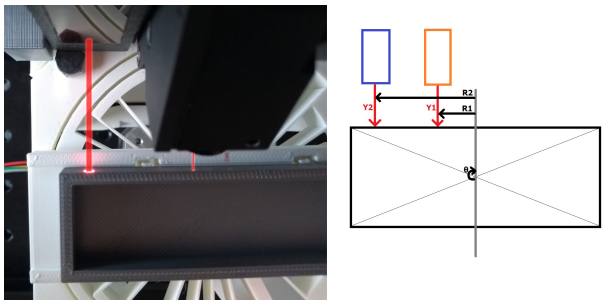

FIG. 26: Precision measurement setup

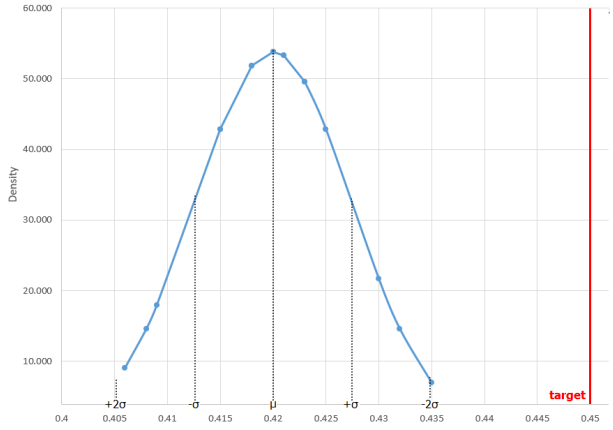

FIG. 27: Normal distribution of the rotational step size

Figure 27 shows the normal distribution of the measured angular step size. The 3σ precision of the step size is 0.02°, with a mean step size of 0.42°, which does not correspond to the expected step size of 0.45°. This might be due to a systematic bias, which slipped into the measurement setup. The actual step size is verified through a different experiment, from which is concluded that the mean step size is in fact 0.45°.

D. Out-of-plane deviation during operation

The slide may not deviate more than $\pm 50\mu m$ in out-of-plane direction, during operation. The setup is shown in figure 28. The linear triangulation sensor is mounted orthogonal the slide surface. The slide surface is covered with white paper, as the transparent glass slide can not be measured on its own.

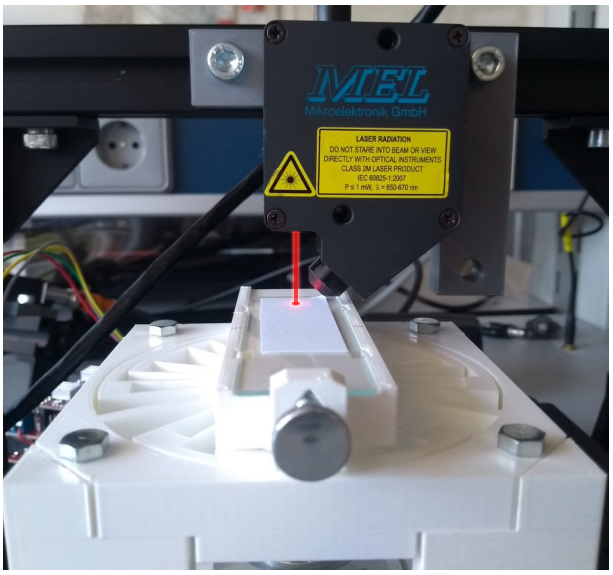

FIG. 28: Setup focus measurement

Figure 29 shows four fine motion stage cycle plots, for which the stage rotates from -20 to +20 steps and back. Each plot corresponds to a different location of the slide along the radial axis. The statistical results are enumerated in table IX.

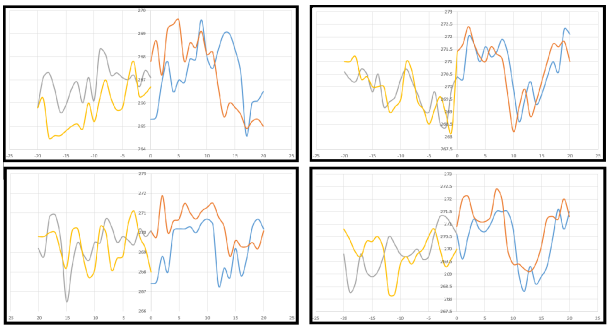

FIG. 29: Cycle plots from -20 steps to + 20 steps

	Mean	Min	Max	Standard deviation	3sigma
Cycle 1	268	266	271	1.3	3.9
Cycle 2	270	268	272	1.0	3.1
Cycle 3	269	267	272	1.1	3.3
Cycle 4	270	268	272	1.0	3.0
Combined	269	266	272	1.4	4.2

TABLE IX: Statistical measures cycle curves

The slide's z-position remains between remains between $\pm 4.2\mu m$ with 99.7% certainty for four cycle plots combined, which is a factor 10 better than the requirements. It is interesting to find out where the error originates from. The graphs do not show a systematic error, but rather a set of random errors. A steady measurement is done, which shows an error with standard deviation

$\sigma_{steady} = 0.5\mu m$. Another significant portion of the error is due to the surface roughness of the paper, which is being measured. The R_a value for commercial printing paper is about 0.94 μm at best [16]. For a Gaussian surface, the standard deviation $\sigma_{surface} = 1.25 * R_a$. If we substitute these values in EQ(6.1), a more realistic standard deviation of the stage performance is obtained. Consequently, the z-position of the slide is estimated to remain within a range of $\pm 2\mu m$ during operation.

$$\sigma_{measured} = \sqrt{(\sigma^2_{sensor} + \sigma^2_{roughness} + \sigma actual)} \quad (6.1)$$

$$\Rightarrow \sigma_{actual} = 0.6\mu m \quad (6.2)$$

VII. DISCUSSION

A. Performance evaluation

The step response measurements proved that the slide stabilizes within the $\pm 1\mu m$ band and that the fine motion stage can operate at 300 ms step interval. The step response does have a relatively large overshoot, which could be reduced with added feed-forward control. This is not yet implemented, as the autofocus time relatively takes the most time (0.5 - 1.0 s), so improved FF control does not add much value. Based on experience with the coarse motion stage, it certainly does not take more time than 10 s to displace the slide one step using the screw. Consequently, the motion scheme can be accomplished within roughly 3 minutes ($300 \cdot 0.3 + 7 \cdot 10 = 160s$). If we take into account the time it takes to perform auto-focus after each step (which takes about 0.5 - 1 s, depending on the phone), the total time for a scan increases to $5-8min$, which is still much faster than the time it takes a trained microscopist to perform the diagnosis by hand (30 - 60 min).

The precision of the coarse motion stage is better than previously desired (30 μm compared to $150\mu m$). Consequently, the step size can be decreased to half a rotation ($250\mu m$ step size), which decreases the workspace from $3.5 \times 8.8mm^2$ to $1.8 \times 8.8mm^2$. The required precision of the fine motion stage is up to par ($0.02° - 11\mu m$). These results ensure that there will be no overlap between images during operation.

An important requirement for the stage is that distance between the smartphone camera and the sample does not change more than $\pm 50\mu m$. This requirement is met by at least a ten-fold. The measured error band was $\pm 4.2\mu m$. If we correct for the inherent measurement uncertainty of the sensor and the surface roughness of the paper, the error band is $\pm 2\mu m$.

B. Robustness evaluation

The worst-case scenario shows that the focus limit and tip/tilt limit will never be exceeded. The costs are kept low, after 200 smear examination, the stage starts to compete with RDT's, which are currently used in the field.

The frame is very unlikely to break down. Although the FMS is designed for infinite life and the CMS is estmated at a long lifetime as well, their lifetime is still uncertain. Only a small portion of the total costs are attributed to the injection molded parts (¡20%), so the FMS and CMS can be replaced if necessary, which are simple procedures. Wear of the screw and nut can occur, but are unlikely, as entire 3D-printers are based on an automated version of this principle (ball screw), which endure exponentially more cycles than this hand-actuated version. The stepper motor is recognized as a robust actuator. It is unsure what the lifetime of the other components, but they can be replaced in a simple manner, if necessary.

The stage is easy to operate, the operator must only align the smear and subsequently rotate the screw 7 times in between cycles. This is much less labor-intensive compared to the conventional manner, where a trained microscopist performs at least 300 actions by hand.

3D-printing or injection molding can be used to fabricate the thermoplastic parts; both are accessible manufacturing technologies. The total number of parts excluding bolts and inserts is 11, which is low. The design is compact: $100 \times 100 \times 80mm^3$. Compactness is evaluated as the area of workspace divided by the planar area of the stage. Its range is $8.8 \times 13mm^2$, thus the compactness is 1.2 %.

VIII. CONCLUSION AND FUTURE RECOMMENDATIONS

In this research, we successfully designed a low-cost, robust and simple planar positioning stage, which meets the requirements for malaria microscopy in field environments. The combination of a stepper motor with a compliant rotary stage and a simple coarse motion stage make it a low-cost, simple and robust design. If one of the components break down, they can easily be replaced. The total costs are relatively low (about $30 for bulk production) and can compete with RDT's after 200 smear examination. The stage completes the operation in about 5 - 8 min (including the autofocus time) and stabilizes well after each step. This is much faster than the time it takes a trained microscopist to perform the diagnosis by hand (30 - 60 min). The step precision of the fine motion stage ($11\mu m$) and coarse motion stage ($30\mu m$) ensure that there is no overlap between images. The focus is ensured, as the slide does not deviate more than $\pm 2\mu m$ in z-direction, during operation, which is more than a ten-fold better than required. For future work, the stepper motor should be replaced 1-on-1 with a me-

chanical variant. In this way, costs can minimized even more and no power source will be required, which is very advantageous for field environments.

[1] C. C. f. D. C. a. Prevention, (2020).
[2] WHO, *World Malaria Report. https://www.who.int/malaria* (World Health Organisation, 2019) p. (accessed 15 Dec. 2019).
[3] CDC - Centers for Disease Control and Prevention, (2020).
[4] WHO, **14**, 29 (2000).
[5] B. A. Mathison and B. S. Pritt, **55**, 2009 (2017).
[6] T. E. Agbana, J. C. Diehl, F. Van Pul, S. M. Khan, V. Patlan, M. Verhaegen, and G. Vdovin, PLoS ONE **13** (2018), 10.1371/journal.pone.0205020.
[7] G. P. Zachary, "Technology alone won't improve health in Africa," (2015).
[8] J. Olberding, B. Williams, A. Schreiner, and J. Paulsen, Quality.
[9] G. Pahl, W. Beitz, J. Feldhusen, and K. H. Grote, *Engineering Design: A Systematic Approach* (Springer London, 2007) pp. 1–617.
[10] Q. Xu, Review of Scientific Instruments **84**, 1 (2013).
[11] J. B. Hopkins and M. L. Culpepper, Precision Engineering **34**, 259 (2010).
[12] A. Mura, A. Ricci, and G. Canavese, Materials **11**, 1 (2018).
[13] M. Galeja, A. Hejna, P. Kosmela, and A. Kulawik, Materials **13** (2020), 10.3390/ma13020297.
[14] J. Sudeepan, K. Kumar, T. K. Barman, and P. Sahoo, International Journal of Applied Engineering Research **9**, 8777 (2014).
[15] I. J. Ezennia, S. O. Nduka, and O. I. Ekwunife, Malaria Journal **16**, 1 (2017).
[16] T. Enomae and F. Onabe, Journal of Fiber Science and Technology **53**, 86 (1997).